Sparsity-Enhanced Optimization for Ejector Performance Prediction

Fenglei Li[a], Changzhi Wu[b,*], Xiangyu Wang[b,c], Qi Tian[a], Kok Lay Teo[d]

[a] *College of Environmental Science and Engineering, Taiyuan University of Technology, Taiyuan, Shangxi 030024,China*
[b] *Australasian Joint Research Centre for Building Information Modelling, School of Built Environment, Curtin University, Perth, WA 6845, Australia*
[c] *Department of Housing and Interior Design, Kyung Hee University, Seoul, Korea*
[d] *Department of Mathematics and Statistics, Curtin University, Perth, WA 6845, Australia*

Abstract

Within a model of the ejector performance prediction, the influence of ejector component efficiencies is critical in the prediction accuracy of the model. In this paper, a unified method is developed based on sparsity-enhanced optimization to determine correlation equations of ejector component efficiencies in order to improve the prediction accuracy of the ejector performance. An ensemble algorithm that combines simulated annealing and gradient descent algorithm is proposed to obtain its global solution for the proposed optimization problem. The ejector performance prediction of a 1-D model in the literature is used as an example to illustrate and validate the proposed method. Tests results reveal that the maximum and average absolute errors for the ejector performance prediction are reduced much more when compared with existing results under the same experimental condition. Furthermore, the results indicate that the ratio of geometric parameters to operating parameters is a key factor affecting the ejector performance.

Keywords: Ejector Performance Prediction; Sparsity-Enhanced Optimization; Global Optimization

1. Introduction

Ejector refrigeration systems (ERSs) have been known since early twentieth century. A study of applying ERS to air-conditioning and refrigeration was reported in mid-1950s. For ERSs, there are many advantages, such as simple construction, high reliability and low maintenance cost in comparison with other refrigeration systems. Although the coefficient of performance (COP) of ERSs is relatively low when compared with that of vapor compression refrigeration systems, ERSs can be powered by low-grade energy, such as solar energy,

*Corresponding author
Email address: c.wu@curtin.edu.au (Changzhi Wu)

Nomenclature

A	Area (m^2)
C_p	specific heat at constant pressure (kJ/kg K)
C_v	specific heat at constant volume (kJ/kg K)
d	diameter (m)
E_r	relative error
m	mass flowrate (kg/s)
M	mach number
P	pressure (MPa)
R	gas constant (kJ/kg K)
T	temperature (K)
u	entrainment ratio
V	velocity (m/s)
η	efficiency relating to isentropic efficiency
ϕ	efficiency account for losses
β	sparsity weight factor
γ	$= C_p/C_v$

Superscripts

c	critical mode of ejector

Subscripts

c	to condenser, exit of ejector
d	diffuser
i	ideal, with no loss
m	mixing flow
p	primary flow, from section1-1 to y-y
p_0	primary flow at inlet of ejector
p_1	primary flow at nozzle exit
r	ratio
s	secondary flow
s_0	secondary flow at inlet of ejector
y	position of the hypothetical throat

Abbreviations

COP	coefficient of performance
ERS	ejector refrigeration system
GDA	gradient descent algorithm
SAA	simulated annealing algorithm
SW	sparsity weight

biomass energy and waste heat. Therefore, there are many research activities on the study of ERSs and their performance in the literature.

For an ERS, it basically consists of a generator, evaporator, condenser, ejector, expansion valve and a pump. The ejector can be regarded as its heart, playing a key role for the performance of the ERS. The ejector design can be classified into two types according to the position of the nozzle [1]: constant-area mixing ejector; and constant-pressure mixing ejector. Both the constant-area mixing model and the constant-pressure mixing model are developed for the prediction of the ejector performance. The predicted results obtained for the constant-area mixing model are found to be consistent with the experimental results. On the other hand, the predicted results obtained for the constant-pressure mixing model do not agree well with the experimental results [2]. However, the performance of a constant-pressure mixing ejector is, in practice, superior to that of a constant-area mixing ejector [3]. Therefore, an intensive effort has been devoted to the study of performance prediction of the constant-pressure mixing ejector. For constant-pressure mixing ejector, there are several models, such as models of Huang et al. [4], Zhu et al. [5] and Chen et al. [6], developed to improve its performance prediction. A 1-D model was proposed in [4] to predict the ejector performance at critical mode with dry refrigerant R141b. It is assumed that the primary flow mixes with the secondary flow under constant-pressure inside the constant-area section of the ejector after the choking of the secondary flow. Four empirical component efficiencies are introduced in the model by

matching the test data. As a result, the prediction accuracy is improved and the prediction results agree well with the experimental data. The maximum relative error on prediction entrainment ratios is -22.99 %. In [5], a model is developed for the ejector performance prediction of both dry and wet refrigerants. The real velocity distribution inside the ejector is approximated by a simple linear function. The mass flow rates of the two flows are derived by intergrading the velocity function at the inlet of the constant-area section. Three empirical component efficiencies are introduced to account for the losses in the ejector. As a result, the maximum relative error is reduced to 13.8 %. In [6], it is assumed that the secondary flow is choking in the hypothetical throat at critical mode and that there is an effective area of the secondary flow at sub-critical mode. Based on the assumptions, the model can predict ejector performance at both critical mode and sub-critical mode with improved prediction accuracy. The maximum relative error on entrainment ratios is 14.2%. It can be seen that the prediction accuracy of these models has been improved by developing novel physical description of the ejector.

In fact, besides the physical description of the ejector, the ejector component efficiencies have dramatic influence on the validity of a 1-D ejector model [7]. The efficiencies are selected as constant value empirically based on experimental date in some cases (e.g. in models of Huang et al. [4] and Eames et al. [8]) or taken from literature in other cases (e.g. in models of Cizungu et al. [9] and yan et al. [10]). However, it is found that ejector component efficiencies relied on the ejector configurations [4] or operating conditions [5] or both of them [11]. Therefore, ejector component efficiencies were presented as empirical correlations in some models, but only empirical methods are introduced to determine the correlation equations of the efficiencies in the models. The question on how to optimize ejector component efficiencies such that simple correlation equations with better prediction accuracy are obtained appears to remain open in the literatures.

The aim of this paper is to develop a unified method to determine correlation equations of ejector component efficiencies in order to pick out and analyze the key factors which affect ejector performance. To begin with, the ejector performance prediction is formulated as a sparsity-enhanced optimization problem [12]. The objective in our optimization problem includes not only the prediction accuracy, but also the number of active terms in the correlation equations. A hybrid algorithm is developed to solve this formulated optimization problem. To illustrate the effectiveness of our proposed method, 1-D model of the ejector performance prediction proposed in [4] is used as an example.

2. Mathematical modelling and optimization formulation

In this section, we will take 1-D model proposed in [4] as an example to illustrate how to formulate the corresponding performance prediction as a sparsity-enhanced optimization problem. The flow characteristic of the model is illustrated in Fig.1.

2.1. Ejector component efficiencies

In order to account for losses at critical mode in ejector, ejector component efficiencies are introduced in most of 1-D ejector models. Four efficiencies, η_p, η_s, ϕ_p and ϕ_m, are taken into consideration in [4]. In the model, the efficiencies, η_p and η_s, relate to the isentropic efficiency of the primary flow from inlet to the nozzle throttle and the secondary flow from inlet to section y-y, respectively. As far as η_p, it is used to account for the loss of the primary flow from section 1-1 to y-y. Huang et al. [4] think the loss may result from the slipping or viscous effect of the primary and the secondary flows at the boundary. However, recent studies have shown that, the loss is due to a series of oblique shocks which the primary flow undergoes as it expands from section 1-1 to y-y [13]. But no matter what reason the loss results from, it can be taken into account by isentropic efficiency.

However, there is some diversity on how to account for losses in the mixing chamber in different ejector models. Huang et al. [4] defined mixing efficiency, ϕ_m, as a momentum transfer efficiency, namely

$$\phi_m = \frac{(m_p + m_s)\, V_m}{m_p V_{py} + m_s V_{sy}} \tag{1}$$

This definition is the same as that in literatures [8**?**]. However, Yu et al. [14] and Xu et al. [15] present another definition of mixing efficiencies, it is

$$\phi_m = \frac{V_m^2}{V_{m,i}^2} \tag{2}$$

Cizungu et al. [16] and Selvaraju and Mani [17] use friction at wall surface of mixing chamber to account for mixing losses. The friction factor f_m is expressed as

$$\frac{1}{\sqrt{f_m}} = 2.0 log\left(Re_m \sqrt{f_m} - 0.8\right) \tag{3}$$

where, Re_m is Reynolds number of mixing flow in the mixing chamber.

2.2. 1-D model: A brief review

The following conditions are assumed to be satisfied.

1. The working fluid is an ideal gas with the properties of C_p and γ being constants;
2. The flow inside the ejector is steady and one dimensional;
3. The kinetic energy of the primary and secondary flow at the inlets and the discharging flow at the outlet are negligible;
4. The isentropic relations are used to approximate the ejector component efficiencies;
5. The primary flow fans out of the nozzle restricting the secondary flow such that they are not mixed until the hypothetical throat of the secondary flow is formed at the cross section y-y.
6. The inner wall of the ejector is adiabatic.

The flow rate m_p of the primary flow at choking condition is given by:

$$m_p = \frac{P_{p0} A_t}{\sqrt{T_{p0}}} \sqrt{\frac{\gamma}{R} \left(\frac{2}{\gamma+1} \right)^{(\gamma+1)/(\gamma-1)}} \sqrt{\eta_p} \tag{4}$$

where, η_p relates to the isentropic efficiency of the primary flow from inlet to nozzle throttle. The parameters M_{p1} and P_{p1} of the primary flow at section 1-1 can be estimated as:

$$\left(\frac{A_{p1}}{A_t} \right)^2 \approx \frac{1}{M_{p1}^2} \left[\frac{2}{\gamma+1} \left(1 + \frac{\gamma-1}{2} M_{p1}^2 \right) \right]^{(\gamma+1)/(\gamma-1)} \tag{5}$$

$$P_{p0}/P_{p1} \approx \left(1 + M_{p1}^2 (\gamma-1)/2 \right)^{\gamma/(\gamma-1)} \tag{6}$$

Then, the pressure at section y-y can be derived as:

$$P_{py} = P_{sy} \approx P_{s0} \left(1 + M_{sy}^2 (\gamma-1)/2 \right)^{\gamma/(1-\gamma)} \tag{7}$$

The Mach number M_{sy} of the primary flow at section y-y is:

$$\frac{P_{py}}{P_{p1}} \approx \frac{\left(1 + \left((\gamma-1)/2 \right) M_{p1}^2 \right)^{\gamma/(\gamma-1)}}{\left(1 + \left((\gamma-1)/2 \right) M_{py}^2 \right)^{\gamma/(\gamma-1)}} \tag{8}$$

By introducing ϕ_p to account for the losses of the primary flow from section 1-1 to section y-y, the area A_{py} occupied by the primary flow at section y-y is:

$$\frac{A_{py}}{A_{p1}} = \frac{(\phi_p/M_{py}) \left[(2/(\gamma+1)) \left(1 + \left((\gamma-1)/2 \right) M_{py}^2 \right) \right]^{(\gamma+1)/(2(\gamma-1))}}{(1/M_{p1}) \left[(2/(\gamma+1)) \left(1 + \left((\gamma-1)/2 \right) M_{p1}^2 \right) \right]^{(\gamma+1)/(2(\gamma-1))}} \tag{9}$$

The area A_{sy} of the secondary flow at section y-y can be calculated as follows:

$$A_{sy} = A_3 - A_{py} \tag{10}$$

It is assumed that the aerodynamic throat of the secondary flow is formed at section y-y, i.e., M_{sy}=1. Then, the mass flow rate of the secondary flow is expressed as given below:

$$m_s = \frac{P_{s0} A_{sy}}{\sqrt{T_{s0}}} \sqrt{\frac{\gamma}{R} \left(\frac{2}{\gamma + 1} \right)^{(\gamma+1)/(\gamma-1)}} \sqrt{\eta_s} \tag{11}$$

where, η_s relates to the isentropic efficiency of the secondary flow from inlet to section y-y. Now the entrainment ratio u, which is the vital parameter of ejector, can be calculated through the following equation.

$$u = m_s / m_p \tag{12}$$

The temperature T_{py} and the velocity V_{py} of the primary flow at section y-y are:

$$T_{p0}/T_{py} = 1 + M_{py}^2(\gamma - 1)/2 \tag{13}$$

and

$$V_{py} = M_{py} \sqrt{\gamma R T_{py}} \tag{14}$$

The temperature T_{sy} and the velocity V_{sy} of the secondary flow at section y-y are:

$$T_{s0}/T_{sy} = 1 + M_{sy}^2(\gamma - 1)/2 \tag{15}$$

and

$$V_{sy} = M_{sy} \sqrt{\gamma R T_{sy}} \tag{16}$$

Both the primary and secondary streams are assumed to have reached the constant pressure, starting to mix at section y-y. The mixing process can be described as:

$$m_p \left(C_p T_{py} + \frac{V_{py}^2}{2} \right) + m_s \left(C_p T_{sy} + \frac{V_{sy}^2}{2} \right) = (m_p + m_s) \left(C_p T_m + \frac{V_m^2}{2} \right) \tag{17}$$

$$\phi_m \left(m_p V_{py} + m_s V_{sy} \right) = (m_p + m_s) V_m \tag{18}$$

where, ϕ_m is the momentum transfer efficiency during the mixing of the two streams. The velocity V_m of the mixed flow is:

$$V_m = M_m \sqrt{\gamma R T_m} \tag{19}$$

The pressure of the mixed flow rises sharply when a supersonic shock takes place at some section after section m-m. Assume that the mixed flow has a uniform pressure after the occurrence of the shock, the pressure P_3 and the Mach number M_3 of the mixed flow follow the gas dynamic relations:

$$P_3/P_m = 1 + (2\gamma/(\gamma+1))\left(M_m^2 - 1\right) \tag{20}$$

$$M_3^2 = \frac{1 + ((\gamma-1)/2)\, M_m^2}{\gamma M_m^2 - (\gamma-1)/2} \tag{21}$$

Now the critical back pressure P_c^c can be derived by using the following equation:

$$P_c^c/P_3 = \left(1 + M_3^2(\gamma-1)/2\right)^{\gamma/(\gamma-1)} \tag{22}$$

2.3. Sparsity-Enhanced Optimization for Ejector Performance Prediction

In the sparsity-enhanced optimization model, it is important to identify critical basis functions which characterize the functional relationship [18]. During the optimization process of the ejector performance prediction, simple expressions of efficiencies can be found while optimizing u and P_c^c by using sparsity-enhanced optimization model. Here, we will formulate the determination of these efficiencies as a sparsity-enhanced optimization problem. In this way, the prediction accuracy is optimized while the most important factors, which affect the prediction accuracy, are also being identified.

Based on the performance prediction model of the ejector described by (4)-(22), the entrainment ratio u and the critical back pressure P_c^c can be expressed as functions of efficiencies $\eta_p, \eta_s, \phi_p, \phi_m$, i.e.,

$$u = u(\eta_p, \eta_s, \phi_p, \phi_m), \quad P_c^c = P_c^c(\eta_p, \eta_s, \phi_p, \phi_m).$$

In the literature, the efficiencies $\eta_p, \eta_s, \phi_p, \phi_m$ appeared in their models of the ejector performance prediction are usually taken as a function of $A_r(= A_3/A_t)$ or/and $P_r(= P_{p0}/P_{s0})$. For example, $\phi_m = 0.9788 - 0.0073A_r$ in [**?**]. However, this relationship is always determined by empirical methods. Thus, there often exists a big gap between experimental results and prediction results. Furthermore, it is time consuming to find out the relationship. In the following, we will develop a unified method to formulate this performance prediction problem as an optimization problem. For this, we suppose that

$$\eta_p = \eta_p(x_p, A_r, P_r),\ \eta_s = \eta_s(x_s, A_r, P_r),\ \phi_p = \phi_p(z_p, A_r, P_r),\ \phi_m = \phi_m(z_m, A_r, P_r), \tag{23}$$

where x_p is the coefficient vector in the correlation equation η_p. For example, it can be assumed that

$$\eta_p = x_{p_1} + x_{p_2}A_r^{-1} + x_{p_3}P_r^{-1} + x_{p_4}(A_r/P_r) + x_{p_5}(A_r/P_r)^{-1} + x_{p_6}(A_rP_r)^{-1}. \tag{24}$$

Similarly, we suppose that

$$\eta_s = \eta_s(x_s, A_r, P_r),\ \phi_p = \phi_p(z_p, A_r, P_r),\ \phi_m = \phi_m(z_m, A_r, P_r), \tag{25}$$

where x_s, z_p and z_m are the corresponding coefficient vectors in the correlation equations. Now the determination of the correlation equations has been transformed into the determination of the coefficient vectors x_p, x_s, z_p and z_m. When no confusion can arise, we rewrite $u(\eta_p, \eta_s, \phi_p, \phi_m)$ and $P_c^c(\eta_p, \eta_s, \phi_p, \phi_m)$ as $u(x_p, x_s, z_p, z_m)$ and $P_c^c(x_p, x_s, z_p, z_m)$, respectively.

Since the losses are between 0 to 1, η_p, η_s, ϕ_p and ϕ_m should satisfy the following constraints:

$$0 \leqslant \eta_p \leqslant 1,\ 0 \leqslant \eta_s \leqslant 1,\ 0 \leqslant \phi_p \leqslant 1,\ 0 \leqslant \phi_m \leqslant 1. \tag{26}$$

Denote

$$E_{u,j}(x_p, x_s, z_p, z_m) = \frac{u_j(x_p, x_s, z_p, z_m) - \hat{u}_j}{\hat{u}_j}, \tag{27}$$

$$E_{P_c,j}(x_p, x_s, z_p, z_m) = \frac{P_{cj}^c(x_p, x_s, z_p, z_m) - \hat{P}_{cj}^c}{\hat{P}_{cj}^c}, \tag{28}$$

$$E_j(x_p, x_s, z_p, z_m) = E_{u,j}^2(x_p, x_s, z_p, z_m) + E_{P_c,j}^2(x_p, x_s, z_p, z_m), \tag{29}$$

$$C(x_p, x_s, z_p, z_m) = \left(\|x_p\|_0 + \|x_s\|_0 + \|z_p\|_0 + \|z_m\|_0\right), \tag{30}$$

where u_j and $\hat{u}_j$ are the jth theoretical calculation and the experimental data of the entrainment ratio, respectively, P_{cj}^c and $\hat{P}_{cj}^c$ are the jth theoretical calculation and the experimental data of the critical back pressure, respectively, $\|\cdot\|_0$ is the number of the non-zero elements of $\cdot$. For example, if $x_p = [0,\ 0.1,\ 0,\ 0.4]$, then $\|x_p\|_0 = 2$. Now the sparsity-enhanced ejector performance prediction can be formulated as the following optimization problem:

$$\min_{x_p, x_s, z_p, z_m} \quad E(x_p, x_s, z_p, z_m) = \sum_{j=1}^{n}(1-\beta)E_j(x_p, x_s, z_p, z_m) + \beta C(x_p, x_s, z_p, z_m), \tag{31}$$

$$s.t. \quad (4) - (30). \tag{32}$$

where β is the sparsity weight (SW) to balance the ejector performance prediction and sparsity, while n is the number of the experimental results. Let this problem be referred to as Problem (P).

2.4. Continuous Approximation

In Problem (P), the cardinality function $C(x_p, x_s, z_p, z_m)$ of x_p, x_s, z_p and z_m is non-continuous. How to solve this optimization problem is challenging. Instead of solving Problem (P) directly, we approximate the cardinality function $C(x_p, x_s, z_p, z_m)$ by 1-norm function. More specifically, $C(x_p, x_s, z_p, z_m)$ is approximated by:

$$\tilde{C}(x_p, x_s, z_p, z_m) = (\|x_p\|_1 + \|x_s\|_1 + \|z_p\|_1 + \|z_m\|_1)\,. \tag{33}$$

Then, this optimization becomes:

$$\min_{x_p, x_s, z_p, z_m} \quad \tilde{E}(x_p, x_s, z_p, z_m) = \sum_{j=1}^{n}(1-\beta)E_j(x_p, x_s, z_p, z_m) + \beta\tilde{C}(x_p, x_s, z_p, z_m), \tag{34}$$

$$s.t. \quad (4) - (29), (33). \tag{35}$$

Let this problem be referred to as Problem (AP). Under certain conditions, we can prove that the solution of Problem (AP) approaches to a solution of Problem (P) [19].

2.5. Smoothing Transformation

The optimization problem defined by (34) and (35) is non-smooth since the absolute value term $\tilde{C}(x_p, x_s, z_p, z_m)$ is involved. It is well-known that the convergence of the optimization process may be slow [20]. Here, we shall transform this non-smooth optimization problem into a smooth optimization problem. For any $x \in \mathbb{R}$, let $|x| = x^+ - x^-$, where $x^+ = \max(x, 0)$ and $x^- = \min(x, 0)$. Replacing $x_{p_i} = x_{p_i}^+ - x_{p_i}^-$, $x_{s_i} = x_{s_i}^+ - x_{s_i}^-$, $z_{p_i} = z_{p_i}^+ - z_{p_i}^-$ and $z_{m_i} = z_{m_i}^+ - z_{m_i}^-$ into (34) and (35), and denoting $X^+ = [x_p^+, x_s^+, z_p^+, z_m^+]^T$, $X^- = [x_p^-, x_s^-, z_p^-, z_m^-]^T$, we obtain the following optimization problem:

$$\min_{X^+, X^-} \quad E(X^+, X^-) = \sum_{j=1}^{n}(1-\beta)E_j(X^+, X^-) + \beta\sum_i \left(X_i^+ + X_i^-\right) \tag{36}$$

$$s.t. \quad (4) - (29), \tag{37}$$

$$X^+ \succeq 0,\ X^- \succeq 0. \tag{38}$$

It can be shown that the optimization problem defined by (36)-(38) is equivalent to that defined by (34) and (35). After the transformation, the original non-smooth optimization problem has been transformed into a smooth one at a cost of doubling the number of variables. In the following section, we will develop a hybrid method to solve this transformed optimization problem.

3. Computational Algorithm

Although the transformed optimization problem is smooth, it is still highly nonlinear and nonconvex. Thus, the optimization problem defined by (36)-(38) may have many local optimal solutions and conventional gradient-based optimization methods may trap into local optimum. In the recent, there are many hybrid algorithms proposed to solve this problem, such as combining meta-heuristic method with local descent methods [21] and combining two deterministic heuristic methods [22]. In this section, we will introduce the hybrid method in [23] through combining simulated annealing method with gradient descent method to solve this optimization problem.

3.1. Gradient Descent Approach

A gradient descent approach (GDA) is much more efficient in local search. The iterative search process at each (or kth) iteration can be expressed as follows:

$$X^+_{i(k+1)} = X^+_{i(k)} - \alpha_k \frac{\partial E_{(k)}}{\partial X^+_{i(k)}},\ X^-_{i(k+1)} = X^-_{i(k)} - \alpha_k \frac{\partial E_{(k)}}{\partial X^-_{i(k)}}. \tag{39}$$

where α_k is the search step size ($\alpha_k > 0$), $E_{(k)} = E(X^+_k, X^-_k)$, $X^+_{i(k)}$ is the ith element of X^+_k and $X^-_{i(k)}$ is the ith element of X^-_k. We set two termination criteria for the search:

(1) If the absolute value, $\left|E_{(k+1)} - E_{(k)}\right|$, of the difference between the two function values at the two successive search steps is smaller than a predefined threshold ε, $X_{st} = X^+_{(k+1)} - X^-_{(k+1)}$ is regarded as the output solution;

(2) If the number of iterative steps is greater than a predefined k_{max}, the iteration terminates.

3.2. Simulated Annealing

Simulated annealing algorithm (SAA) is a kind of metaheuristic methods [24] which was originally developed in [25] and [26]. It can explore the function's entire surface during the optimization by uphill and downhill moves, escape from local minima and go on to find a global minimum. In our problem, SAA is used to find a better initial solution for GDA. SAA will search from the current solution $X_{(0)}$ obtained by GDA to search for a better solution X_{st} in the range from the initial annealing temperature T_b to the termination annealing temperature T_f. The iterative search process at each temperature T can be expressed as follows:

Set initial location $X_{(0)}$ and let it be the current location $X_{(c)}$. Based on it, generate a subsequent location $X_{(s)}$ by applying a perturbation mechanism using s as a step. If the difference, D, between $E(X^+_{(s)}, X^-_{(s)})$ and $E(X^+_{(c)}, X^-_{(c)})$ is less than 0, or $min(1, exp(D/T))$ is larger than a random number ξ_0 in [0,1], the subsequent location $(X^+_{(s)}, X^-_{(s)})$ is accepted as the new current location $(X^+_{(c)}, X^-_{(c)})$ to perform the next search. For each temperature T, the iteration operates N times, then T is reduced by cooling speed factor λ. The termination criteria is: If T is not higher than the termination annealing temperature T_f, the current location is regarded as the estimated location X_{st}.

3.3. Hybrid Global Optimization Algorithm

Although SAA has very nice convergent property and can escape from local minima, sometimes the global minimum with pre-defined precision will cost a large amount of computation time [27]. However GDA approach can quickly converge to a local optimization solution with high accuracy. Therefore, a hybrid global optimization algorithm is developed by combining SAA with GDA. SAA is used to find a global initial optimum, escaping from local minima. Then, GDA is used to accelerate the convergence to the optimum. The hybrid algorithm is a much more efficient to search for a global solution of the optimization problem (36)-(38). The process of the algorithm is illustrated in Fig.2.

4. Results and Discussions

In this section, we will use our developed method to determine the correlation equations, compare the results obtained by our method with those obtained by existing methods and analyze influence of the key parameters picked out by our method on ejector performance. Here, we will use the experimental data reported in [4] for validation and comparison. The experiments are carried out for 11 different ejectors at 39 critical-mode operation points. The area ratio A_r and the pressure ratio P_r range from 6.44 to 10.64 and from 8.51 to 15.1, respectively.

4.1. Correlation Equations

Now we first use our proposed method to determine correlation equations of ejector component efficiencies. Since the efficiencies are non-dimensional quantities, the correlations should be functions of non-dimensional parameters. Area ratio, A_r, is an important non-dimensional parameter affecting ejector

performance [28] and the efficiencies [4]. Therefore, A_r is selected as a non-dimensional parameter in the correlation equations. It is known that the information of downstream cannot travel back to the upstream and the entrainment ratios remain constant at critical mode [29]. Thus, besides the area ratio, A_r, the efficiencies and the ejector performance are mainly affected by the pressure, P_{p0} and P_{s0}. Then, non-dimensional parameter $P_r(= P_{p0}/P_{s0})$ is selected as another parameter.

Hence, most of the correlation equations, such as those in literature [**?**] and [11], are supposed as the functions of A_r and P_r. Here, the correlation equations are taken as in the form of (24), where each of the components is determined through six coefficients. In our method, β is a key factor influencing the results in the performance prediction of the ejector. However, a suitable value of β is unknown and thus it was taken from 0 to 0.9 with step of 0.1 in calculation so as to obtain the best result. During the solution process, we observe that the optimization problem can achieve a good trade-off between the sparsity of coefficient vectors x_p, x_s, z_p, z_m and the prediction performance at $\beta = 0.8$. The corresponding correlation equations obtained are as given below:

$$\eta_p = 0.9490 + 0.0037(A_r/P_r), \tag{40}$$

$$\eta_s = 0.8453 + 0.0028(P_r/A_r), \tag{41}$$

$$\phi_p = 0.9610 + 0.1144(A_r/P_r) - 0.0971(P_r/A_r), \tag{42}$$

$$\phi_m = 0.8452 - 0.0281(A_r/P_r) + 0.0578(P_r/A_r). \tag{43}$$

The correlation equations (40)-(43) determined by our method only include the terms containing A_r/P_r or/and P_r/A_r besides the constant term. Moreover, the coefficients of A_r/P_r or P_r/A_r in the correlation equations of η_p and η_s are much less than those of ϕ_p and ϕ_m. Therefore, A_r/P_r and P_r/A_r have more influence on ϕ_p and ϕ_m than η_p and η_s. Because the ejector component efficiencies have significant effect on the ejector performance , A_r/P_r and P_r/A_r will influence the ejector performance eventually. On the other hand, we note that the term A_r^{-1} and P_r^{-1} are removed from the original candidate correlation equations (24) after optimization. This is due to the action of sparsity-enhanced optimization. Thus, integrating A_r and P_r as A_r/P_r or P_r/A_r to analyze the ejector performance is more efficient than only using A_r and P_r. For convenience, we define A_r/P_r as the ratio of geometric parameters to operating parameters, and P_r/A_r as the ratio of operating parameters to geometric parameters.

It should be noted that the correlation equations of the efficiencies were determined based on the experimental data in [4]. Thus, they should be used within the following boundaries which are the same as those of experimental data:

$$0.400MPa \leqslant P_{p0} \leqslant 0.604MPa,\ 0.040MPa \leqslant P_{s0} \leqslant 0.047MPa, \tag{44}$$

$$6.44 \leqslant A_r \leqslant 10.64,\ for\ 2.64mm \leqslant A_t \leqslant 2.82mm, \tag{45}$$

$$0.426 \leqslant A_r/P_r \leqslant 1.106 \tag{46}$$

Besides the operating parameters and geometric parameters as shown in (44) to (46), material used and manufacturing techniques, such as machining, interior surface polishing, also have influence on the ejector component efficiencies. From this viewpoint, the 1-D model can be treated as a semi-empirical model [4]. Thus, when operating parameters and/or geometric parameters are out of the boundaries or material used and manufacturing techniques are different from the test ejectors, the correlation equations of the efficiencies should be determined according to the new test data. Obtaining simple correlation equations with better prediction accuracy and less calculation times is the merit of our unified method. Clearly, our method makes it easier for such 1-D ejector models to be used in the industry.

4.2. Comparisons with Existing Results

There are two different methods to improve the performance prediction of the ejector. One is to build a better model and the other one is to find a better correlation equations of ejector component efficiencies. No matter what method is used, the goal is to improve the prediction accuracy. Now we compare our results obtained by the correlation equations given in (40)-(43) with those reported in [4], [5] and [6]. The error results $E_{u,j}$ in (27) for the entrainment ratio u are reported in Table 1. It can be observed that the maximum error is 7.03% using our proposed correlation equations which is significant better than -22.99% in [4]. The average absolute error $\frac{1}{n}\sum_{j=1}^{n}|E_{u,j}|$ is 2.82% obtained by our method, which is much better than 8.70% in [4]. Thus, both maximum error and average absolute error are reduced significantly by using our ejector component efficiencies in the model reported in [4].

Now we compare our results with those in [5] and [6]. The model reported in [5] is proposed to predict the performance for both dry and wet refrigerant and the model reported in [6] is used to estimate performance

at critical and sub-critical modes. It can be seen that the prediction accuracy of the model is better than that in [4]. However, the maximum errors reported in [5] and [6] are still larger than 10% since the ejector component efficiencies have not been optimized as what we do. More precisely, they are 13.80% in [5] and -14.20% in [6], respectively.

It is obvious that, after the ejector component efficiencies being optimized by our method, the prediction accuracy of the model in [4] is much better than those reported in [5] and [6] under the same experimental settings. Thus, our method can improve the prediction accuracy of the ejector models significantly. It can be expected that the prediction accuracy of the models in [5] and [6] can be improved by optimizing the ejector component efficiencies using our method.

Note that the results in [30] are not listed in Table 1 for comparison although the entrainment ratios u, which are under the same operating parameters and geometric parameters as in Table 1, are available there. This is because the authors in [30] adopt a piecewise analysis method while we adopt a basis selection method. More specifically, in [30], a trial-and-error method is applied to try different values of mixing efficiency ϕ_m and diffuser efficiency η_d so that both u and A_r get close to the experimental data (error $< 2.5\%$) for 39 experimental points. Then, a regression method is introduced to determine the correlation equations. The method does produce promising results in [30]. However, the values of the coefficient of determination (R^2) are not equal to 1 for the correlation equations of ejector component efficiencies [30] and the entrainment u obtained by the correlation equations is not available in [30]. Moreover, the correlation equations involve many more terms than those obtained by our method. For example, $\phi_m = 6.7837+0.1611(P_{p0}/P_c)^2-2.6404(P_{p0}/P_c)+0.1924(P_c/P_{s0})^2-2.4919(P_c/P_{s0})-0.0123P_r^2+0.6634P_r-0.0172A_r^2+0.3479A_r+0.1611u^2+0.3767u$. In comparison, our method can optimize the prediction accuracy while minimizing the number of terms in (24). If the predicted error is the only pursuit without sparsity consideration, our method can achieve better results just by setting $\beta = 0$ and using the forms as in [30] for regression.

A comparison of the results for the critical back pressure P_c^c obtained by our method and those obtained by experiments reported in [4] is shown in Fig. 3. It can be observed that the prediction results coincide fairly well with the experimental data within $\pm 6\%$ error. Indeed, the relative errors of P_c^c are so small that the average absolute error $\frac{1}{n}\sum_{j=1}^{n}|E_{P_c,j}|$ is 1.5%.

4.3. Analysis of Ejector Performance

From the reported results in equation (40)-(43), the key factors affecting the ejector performance prediction are A_r/P_r and P_r/A_r. Therefore, analyzing effects of A_r and P_r on ejector performance simultaneously should be more significant.

Fig. 4 illustrates the effects of area ratio A_r and pressure ratio P_r on the entrainment ratio u. It can be observed that u increases as A_r increase and P_r decrease. Hence, the maximum u is achieved when $A_r = 10$ and $P_r = 10$, while the minimum u is achieved when $A_r = 7$ and $P_r = 15$. Although a large u is good for the performance of ejector system, the critical back pressure P_c^c, which corresponds to u, should be higher than the condensation pressure P_c provided by the condenser. Compared with u, P_c^c varies inversely with A_r and P_r, as shown in Fig. 5. Therefore, for a given u, we should adjust A_r and P_r to ensure $P_c^c \geqslant P_c$.

The variation of u and COP of ejector system with A_r/P_r when $P_c^c = 0.116$MPa are illustrated in Fig. 6 and Fig. 7, respectively. The figures show that both u and COP are positively correlated with A_r/P_r at a fixed pressure of the secondary flow at the inlet of the ejector, P_{s0}. It can also be observed that u and COP at low P_{s0} are lager than those at high P_{s0} for the same value of A_r/P_r, which indicates that the performance of ejectors at low P_{s0} is better than that at high P_{s0} under this condition. Because P_c^c is at the same value, the pressure of the primary flow at the inlet of ejector, P_{p0}, is higher for lower P_{s0}. Thus, P_r is larger. This indicates that A_r is larger for the same value of A_r/P_r. In conclusion, the performance of ejectors under low P_{s0} is better than that under high P_{s0} at the expense of higher values of A_r and P_r. It can be seen that the values of COP are slightly lower than u under the same operating condition. Further observation reveals that the increasing rates of COP are lower than those of u when A_r/P_r increases.

Fig. 8 and Fig. 9 describe the variations of P_c^c and COP of the ejector system against A_r/P_r when $u = 0.4$. It can be observed in Fig. 8 that P_c^c decreases with the increase of A_r/P_r for each fixed P_{s0}. In fact, the decrease of P_c^c is caused by the decrease of P_{p0} when P_{s0} is fixed. Furthermore, the decrease of P_{p0} will result in the decrease of P_r. In return, A_r/P_r will increase. Therefore, P_{p0} should be reduced and A_r should be increased in order to maintain u being a constant when A_r/P_r increases. Assuming the losses of the pipes from the generator, evaporator and condenser to the ejector are negligible, COP can be expressed as:

$$COP = (h_{s0} - h_c)/(h_{p0} - h_c) \tag{47}$$

where h_{p0} and h_{s0} are enthalpies of the primary flow and the secondary flow at the inlet of the ejector, respectively; h_c is the enthalpy of the mixed flow which has been condensed by the condenser. Eq. (47) indicates that, for fixed h_{s0}, the decreases of h_c and h_{p0} will increase COP since h_{s0} is lower than h_{p0}. According to Fig. 8, P_c^c and P_{p0} decrease with the increase of A_r/P_r. Therefore, COP will increase with the increase of A_r/P_r. This trend is depicted in Fig. 9.

5. Conclusions

A novel sparsity-enhanced optimization method was proposed to determine the correlation equations of ejector component efficiencies in order to improve the prediction accuracy of the ejector performance. Through introducing sparsity penalty term, the method can identify critical factors which have dominating influence on the prediction accuracy of ejector performance. The combined method of simulated annealing and gradient descent algorithm shows potential to find a global optimal solution to the formulated optimization problem. The results obtained by the method improves the performance prediction accuracy of ejector model significantly over the existing empirical based methods. The ejector component efficiencies in a typical ejector model have been optimized by the methods and the result indicates that the average absolute error and the maximum error have been improved from 8.70% to 2.82% and from -22.99% to 7.03%, respectively. It is also found that the ratio of geometric parameters to operating parameters is a key factor affecting the ejector component efficiencies and ejector performance.

Acknowledgement

This research is supported by International Science and Technology Cooperation Project of China (2013DFA61580), Key Science and Technology Program of Shanxi Province, China (20140313006-6), the Natural Science Foundation of China (61473326, 50976074), the Natural Science Foundation of Chongqing (cstc2013jjB00001 and cstc2013jcyjA00029) and Australasian Joint Research Centre for Building Information Modelling.

[1] Sun D W, Eames I W. Recent developments in the design theories and application of ejectors: a review. Journal of the Institute of Energy, 1995, 68: 65-79.

[2] Keenan, Joseph Henry. An investigation of ejector design by analysis and experiment. Journal of Applied Mechanics 1950, 17: 299.

[3] Yapici R, Ersoy H K. Performance characteristics of the ejector refrigeration system based on the constant area ejector flow model. Energy Conversion and Management, 2005, 46: 3117-3135.

[4] Huang B J, Chang J M, Wang C P, Petrenko V A. A 1-D analysis of ejector performance. International Journal of Refrigeration, 1999, 22: 354-364.

[5] Zhu Y, Li Y. Novel ejector model for performance evaluation on both dry and wet vapors ejectors. International Journal of Refrigeration, 2009, 32: 21-31.

[6] Chen W, Liu M, Chong D, Yan J, Little A B, Bartosiewicz Y. A 1D model to predict ejector performance at critical and sub-critical operational regimes. International Journal of Refrigeration, 2013, 36: 1750-1761.

[7] Varga S, Oliveira A C, Diaconu B. Numerical assessment of steam ejector efficiencies using CFD. international journal of refrigeration, 2009, 32(6): 1203-1211.

[8] Eames I W, Aphornratana S, Haider H. A theoretical and experimental study of a small-scale steam jet refrigerator. International Journal of Refrigeration, 1995, 18(6): 378-386.

[9] Cizungu K, Groll M, Ling Z G. Modelling and optimization of two-phase ejectors for cooling systems. Applied thermal engineering, 2005, 25(13): 1979-1994.

[10] Yan G, Bai T, Yu J. Thermodynamic analysis on a modified ejector expansion refrigeration cycle with zeotropic mixture (R290/R600a) for freezers. Energy, 2016, 95: 144-154.

[11] Liu F, Groll E A, Li D. Investigation on performance of variable geometry ejectors for CO2 refrigeration cycles. Energy, 2012, 45: 829-839.

[12] Bahmani S. Sparsity-Constrained Optimization//Algorithms for Sparsity-Constrained Optimization. Springer International Publishing, 2014: 11-35.

[13] Bartosiewicz Y, Mercadier Y, Proulx P. Numerical investigations on dynamics and heat transfer in a turbulent underexpanded jet. AIAA journal, 2002, 40(11): 2257-2265.

[14] Yu J, Ren Y, Chen H, et al. Applying mechanical subcooling to ejector refrigeration cycle for improving the coefficient of performance. Energy Conversion and Management, 2007, 48(4): 1193-1199.

[15] Xu X X, Liu C, Fu X, et al. Energy and exergy analyses of a modified combined cooling, heating, and power system using supercritical CO2. Energy, 2015, 86: 414-422.

[16] Cizungu K, Mani A, Groll M. Performance comparison of vapour jet refrigeration system with environment friendly working fluids. Applied Thermal Engineering, 2001, 21(5): 585-598.

[17] Selvaraju A, Mani A. Analysis of a vapour ejector refrigeration system with environment friendly refrigerants. International Journal of Thermal Sciences, 2004, 43(9): 915-921.

[18] Fan C, Huang Y, Wang Q. Sparsity-promoting polynomial response surface: A new surrogate model for response prediction. Advances in Engineering Software, 2014, 77: 48-65.

[19] Bruckstein A M, Donoho D L, Elad M. From sparse solutions of systems of equations to sparse modeling of signals and images, SIAM review, 2009, 51: 34-81.

[20] Long Q, Wu C, Wang X. A system of nonsmooth equations solver based upon subgradient method. Applied Mathematics and Computation, 2015, 251: 284-299.

[21] Long Q, Wu C. A hybrid method combining genetic algorithm and Hooke-Jeeves method for constrained global optimization, Journal of Industrial and Management Optimization, 2014, 10(4): 1279-1296.

[22] Zhang T, Zhang Y J, Zheng Q P, et al. A hybrid particle swarm optimization and tabu search algorithm for order planning problems of steel factories based on the Make-To-Stock and Make-To-Order management architecture. Journal of Industrial and Management Optimization, 2011, 7(1): 31.

[23] Yiu K F C, Liu Y, Teo K L. A hybrid descent method for global optimization. Journal of Global Optimization, 2004, 28: 229-238.

[24] Liu J, Teo K L, Wang X, Wu C. An exact penalty function-based differential search algorithm for constrained global optimization. Soft Computing, 2015: 1-9.

[25] Kirkpatrick S, Vecchi M P. Optimization by simmulated annealing. Science, 1983, 220: 671-680.

[26] Cerny V. Thermodynamical approach to the traveling salesman problem: An efficient simulation algorithm. Journal of Optimization Theory and Applications, 1985, 45: 41-51.

[27] Long Q, Wu C, Huang T, Wang, X. A genetic algorithm for unconstrained multi-objective optimization. Swarm and Evolutionary Computation, 2015, 22: 1-14.

[28] Chen X, Omer S, Worall M, et al. Recent developments in ejector refrigeration technologies. Renewable and Sustainable Energy Reviews, 2013, 19: 629-651.

[29] Chong D, Hu M, Chen W, et al. Experimental and numerical analysis of supersonic air ejector. Applied Energy, 2014, 130: 679-684.

[30] Chen J, Havtun H, Palm B. Parametric analysis of ejector working characteristics in the refrigeration system. Applied Thermal Engineering, 2014, 69: 130-142.

Table 1: Results of 1-D model by our proposed method, Huang et al.(1999), Zhu et al.(2009) and Chen et al.(2013).

A_3/A_t	T_{p0} (℃)	T_{s0} (℃)	Experiment u	Huang et.al u	present u	Huang et.al $E_{u,j}$	Zhu et. al $E_{u,j}$	Chen et.al $E_{u,j}$	present $E_{u,j}$
AA Ejector									
6.44	95	8	0.1859	0.1554	0.1836	-16.43	-0.78	-14.20	-1.25
6.44	90	8	0.2246	0.2156	0.2196	-3.99	1.55	-8.73	-2.25
6.44	84	8	0.2880	0.2880	0.2736	0.23	1.53	-6.08	-5.01
6.44	78	8	0.3257	0.3525	0.3406	8.24	13.80	7.18	4.57
6.44	95	12	0.2350	0.2573	0.2359	9.49	7.04	-4.26	0.39
6.44	90	12	0.2946	0.3257	0.2805	10.54	3.50	-5.40	-4.78
6.44	84	12	0.3398	0.4147	0.3465	22.04	12.58	4.74	1.98
AB Ejector									
6.99	90	8	0.2718	0.2093	0.2559	-22.99	-2.80	-8.65	-5.85
6.99	84	8	0.3117	0.3042	0.3167	-2.39	6.90	2.73	1.60
6.99	78	8	0.3922	0.4422	0.3915	12.74	6.32	3.60	-0.17
AG Ejector									
7.73	95	8	0.2552	0.2144	0.2588	-15.98	2.21	-1.84	1.42
7.73	90	8	0.3040	0.2395	0.3061	-21.22	2.70	0.82	0.68
7.73	84	8	0.3883	0.3704	0.3758	-4.61	-0.20	-0.33	-3.22
7.73	78	8	0.4393	0.4609	0.4610	4.93	8.97	10.02	4.94
7.73	95	12	0.3503	0.3434	0.3274	-1.97	-2.96	-5.48	-6.55
7.73	90	12	0.4034	0.4142	0.3847	2.67	-0.49	-1.59	-4.63
7.73	84	12	0.4790	0.4769	0.4686	12.09	2.86	2.65	-2.18
7.73	78	12	0.6132	0.6659	0.5703	8.60	-2.00	-1.34	-7.00
AC Ejector									
8.28	95	8	0.2814	0.2983	0.2921	6.01	4.25	2.99	3.82
8.28	90	8	0.3488	0.3552	0.3441	1.84	-0.22	0.43	-1.35
8.28	84	8	0.4241	0.4605	0.4204	8.58	0.94	3.11	-0.88
8.28	78	8	0.4889	0.5966	0.5132	22.03	7.35	10.72	4.98
AD Ejector									
9.41	95	8	0.3457	0.3476	0.3622	0.56	3.64	6.83	4.78
9.41	90	8	0.4446	0.4178	0.4236	-6.02	-5.62	-1.26	-4.71
9.41	84	8	0.5387	0.5215	0.5132	-3.19	-5.50	0.06	-4.73
9.41	78	8	0.6227	0.6944	0.6216	11.51	-0.91	5.77	-0.17
9.41	95	12	0.4541	0.4708	0.4512	3.67	-0.29	3.46	-0.64
9.41	90	12	0.5422	0.5573	0.5247	2.78	-2.85	1.73	-3.23
9.41	84	12	0.6350	0.6906	0.6313	8.75	-0.20	5.37	-0.59
9.41	78	12	0.7412	0.8626	0.7596	16.37	2.76	9.21	2.48
EG Ejector									
6.77	95	8	0.2043	0.1919	0.2023	-6.06	0.06	-10.38	-0.96
EC Ejector									
7.26	95	8	0.2273	0.2078	0.2309	-8.57	2.68	-4.27	1.56
7.26	95	12	0.3040	0.3235	0.2936	6.41	1.36	-3.72	-3.43
ED Ejector									
8.25	95	8	0.2902	0.2658	0.2903	-8.39	0.35	-1.03	0.04
EE Ejector									
9.17	95	8	0.3505	0.3253	0.3472	-7.20	-1.75	0.49	-0.94
9.17	95	12	0.4048	0.4894	0.4333	10.55	7.87	11.12	7.03
EF Ejector									
9.83	95	8	0.3937	0.3774	0.3887	-4.13	-3.01	1.22	-1.27
9.83	95	12	0.4989	0.5482	0.4827	9.89	-3.77	0.98	-3.25
EH Ejector									
10.64	95	8	0.4377	0.4627	0.4403	5.70	-2.19	4.20	0.59

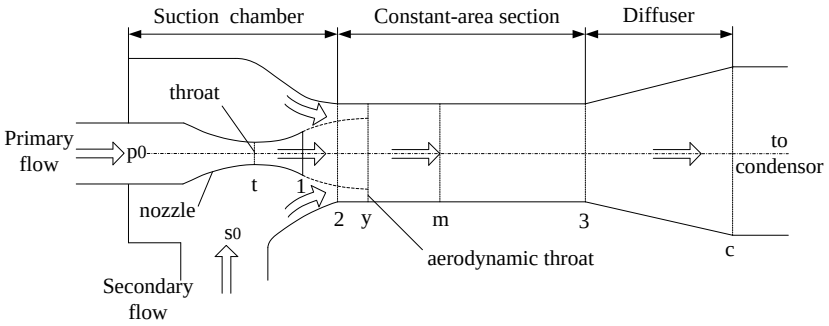

Figure 1: Schematic diagram of ejector

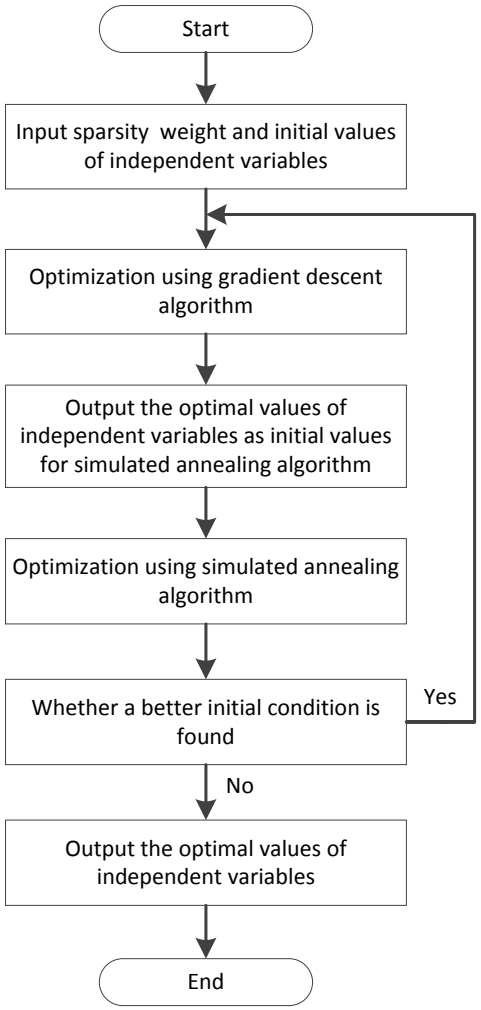

Figure 2: Flow chart of hybrid global optimization algorithm

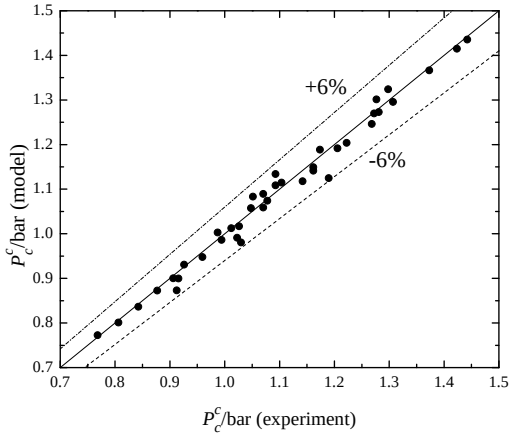

Figure 3: Predictive critical back pressure v.s experimental critical back pressure

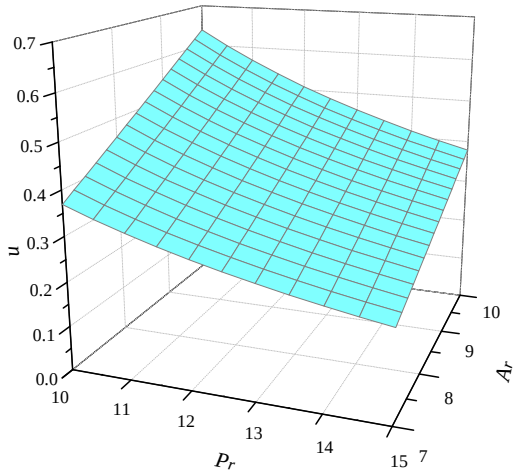

Figure 4: Variation of entrainment ratio with area ratio and pressure ratio

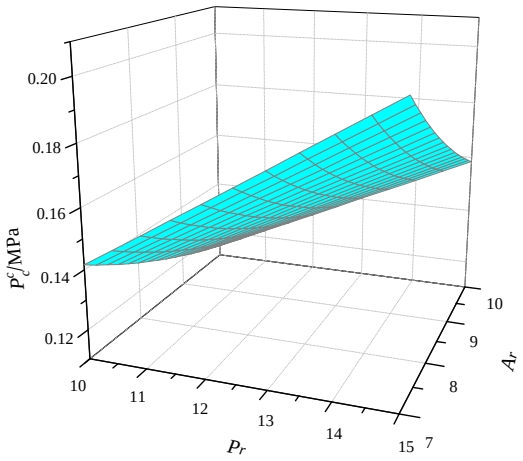

Figure 5: Variation of critical back pressure with area ratio and pressure ratio

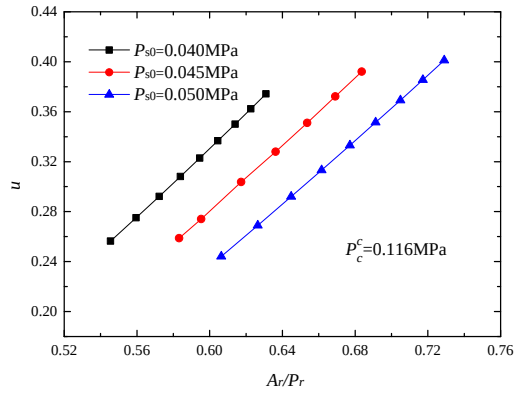

Figure 6: Effects of A_r/P_r on entrainment ratio at critical back pressure equalling 0.116MPa

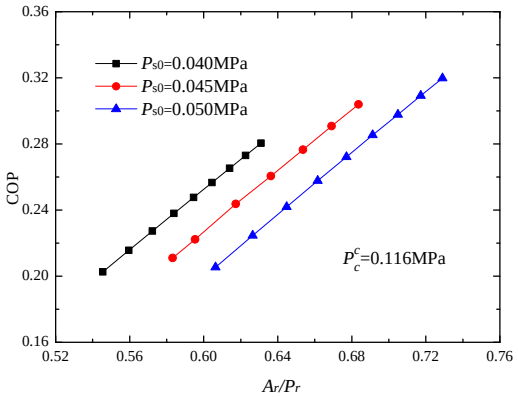

Figure 7: Effects of A_r/P_r on the coefficient of performance at critical back pressure equalling 0.116MPa

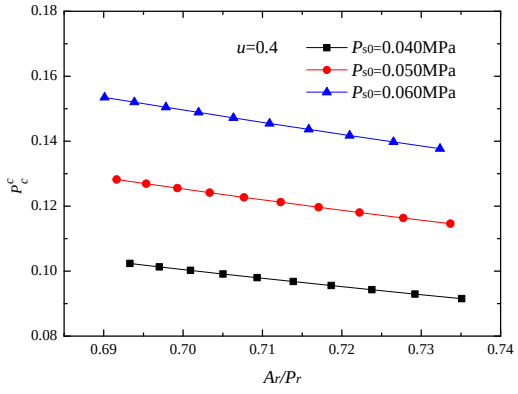

Figure 8: Effects of A_r/P_r on critical back pressure for entrainment ratio equal to 0.4

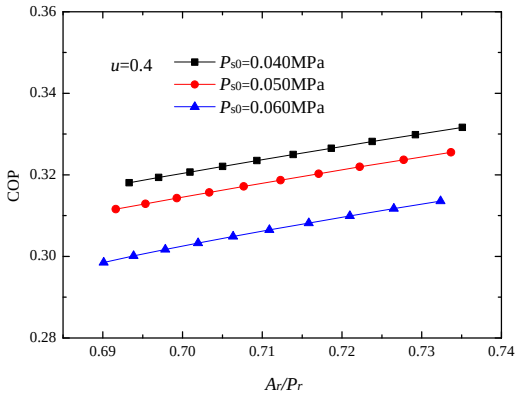

Figure 9: Effects of A_r/P_r on the coefficient of performance for entrainment ratio equal to 0.4